Journal of Magnetism and Magnetic Materials 421 (2017) 250–259

Contents lists available at ScienceDirect

Journal of Magnetism and Magnetic Materials

journal homepage: www.elsevier.com/locate/jmmm

Influence of shear cutting parameters on the electromagnetic properties of non-oriented electrical steel sheets

H.A. Weiss [a,*], N. Leuning [b], S. Steentjes [b], K. Hameyer [b], T. Andorfer [a], S. Jenner [a], W. Volk [a]

[a] Institute of Metal Forming and Casting, Technical University of Munich, Garching, D-85748 Germany
[b] Institute of Electrical Machines, RWTH Aachen University, Aachen, D-52062 Germany

ARTICLE INFO

Article history:
Received 30 June 2016
Accepted 2 August 2016
Available online 6 August 2016

Keywords:
Non-oriented electrical steel
Shear cutting
Residual stress distribution
Micro hardness
Cutting surface parameters
Magnetic properties

ABSTRACT

Mechanical stress occurring during the manufacturing process of electrical machines detrimentally alters the magnetic properties (iron losses and magnetizability). This affects the efficiency and performance of the machine. Improvement of the manufacturing process in terms of reduced magnetic property deterioration enables the full potential of the magnetic materials to be exploited, and as a result, the performance of the machine to be improved. A high quantity of electrical machine components is needed, with shear cutting (punching, blanking) being the most efficient manufacturing technology. The cutting process leads to residual stresses inside the non-oriented electrical sheet metal, resulting in increased iron losses. This paper studies the residual stresses induced by punching with different shear cutting parameters, taking a qualitative approach using finite element analysis. In order to calibrate the finite element analysis, shear cutting experiments are performed. A single sheet tester analysis of the cut blanks allows the correlation between residual stresses, micro hardness measurements, cutting surface parameters and magnetic properties to be studied.

1. Introduction

Manufacturing the core of electrical machines affects the magnetic properties of the electrical steel sheets in terms of the deterioration of energy loss and magnetizability. The degraded magnetic properties, compared to those obtained by standardized metrological measurements carried out on the cold-rolled product, directly affect the efficiency and performance of the electrical machines. Among the different steps from the raw material to the final assembled electrical machine, the shape-giving process is critical to magnetic property deterioration.

In this regard, one possible means of reducing the power loss of an electrical machine is to improve the manufacturing process of the electromagnetic components. Two main components used in nearly every electrical machine are the stator and rotor cores, which are made from stacked non-oriented electric steel sheets. Shear cutting (punching, blanking) and laser cutting are the two most commonly-used manufacturing technologies. While laser cutting is often deployed within the construction of a prototype, shear cutting is used to manufacture large numbers of components. No matter which of these two manufacturing methods is used, the materials' magnetic properties are altered [1]. This is caused by an increasing amount of residual stress induced near the cutting edge. Although investigations have been undertaken using magneto-optical Kerr effect [2] or neutron grating interferometry (nGI) [3] to identify the residual stress penetration depth away from the cutting edge, the residual stress distribution in the zone affected by shear cutting (ZASC) is unknown.

Each processing step in a manufacturing chain leads to residual stresses inside a material [4]. Consider a punching process – the material failure occurs when the shear fracture limit due to high work hardening is reached. The strain induced by the high deformation causes stress in the ZASC. Even once the parts have been cut and all external loads have been removed, the strains are still present. The stress left in the material is known as residual stress. When an electrical steel sheet affected by residual stress is magnetized, the stress prevents the magnetic domains from being aligned in the direction of the external magnetic field [5]. The extent of this effect is determined by the magnitude of the residual stress [6,7].

Besides the magnitude of residual stress, the penetration depth of the ZASC also has an impact on the overall specific losses. In particular, on a stator tooth of small electric machines, the ZASC of both tooth sides can overlap. Depending on the electrical steel material used, the degraded zone may extend up to 15 mm away from the cut edge [8]. Whereas [9] postulated that the affected area is less than 10 mm wide, [10] measures a penetration depth of 0.4 mm for the ZASC using nanoindentation.

* Corresponding author.
E-mail address: hw@utg.de (H.A. Weiss).

http://dx.doi.org/10.1016/j.jmmm.2016.08.002
0304-8853/

The influence of sharp and blunt cutting tools on the magnetic properties is studied in [11]. Increasing wear on the cut edge results in higher specific losses. According to [12], a small distance between the punch and the die implicates better magnetic properties than a large distance when a guillotine is used to separate electrical steel sheets. The distance between the two cutting elements is also known as cutting clearance (CCL). [13] investigates the effect of shear cutting with different CCLs and tool wear states using an industrial cutting tool. The cut specimens are examined with an Epstein frame. This shows that higher cutting clearances and increasing tool wear lead to higher specific losses.

The influence of an increase in volume affected by residual stresses has also been investigated with a single sheet tester for guillotining [14] and for industrial shear cutting [15]. Both studies confirm the results of the Epstein frame tests, where an increasing cutting line length, i.e. volume of the ZASC, results in higher specific losses.

The aim of this paper is to show the coherence between electromagnetic properties and residual stress states that originate from cutting with different process parameters. Therefore, specimens are cut using an industrial shear cutting tool. The specimens are analyzed with regard to their geometrical and mechanical cutting influence using tactile and micro hardness measurement systems. Single sheet tests of the processed electrical steel sheets are performed to identify the magnetic properties for each parameter variation. To identify the magnitude and distribution of the residual stresses in the ZASC for varying shear cutting parameters and blank thicknesses, a finite element analysis (FEA) of the shear cutting process is carried out. In order to do this, the material has to be mechanically characterized. To ensure a good quality of the FEA, the virtual results are correlated with shear cutting experiments using the same cutting parameters. The experimental as well as the virtual results are compared with each other in order to find a correlation between residual stresses, hardness measurements, cutting surface parameters and magnetic properties.

2. Materials

This paper studies two electrical steel grades, material A and material B, with a silicon content of 2.4 wt% and a thickness s_0 of 0.35 and 0.5 mm. Both materials are produced by the same hot-rolled material. The material is quantified using a spark spectrometer. The chemical composition is shown in Table 1. Optical micrographs of the electrical steel sheet both in the direction of and perpendicular to the rolling direction (RD) show that the tempering of the material has led to equiaxed grains with a slightly smaller average grain size for material A (Fig. 1). The number of grains over the sheet metal thickness and the values obtained from the micro hardness analysis can be found in Table 2.

The small number of grains across the sheet thickness is characteristic for non-oriented electrical sheet metal. After cold rolling and tempering, the material is coated with an organic EC3 coating. A comparison between the coated and non-coated material determined that there is neither a difference in grain size nor in the material's micro hardness.

For the FEA, it is necessary to know the stress-strain behavior of the material. Therefore, uniaxial tension tests according to [16] were carried out. In addition to the tension tests in 0°, 45° and 90° to RD, the experiments were also carried out using higher tension speeds v_t of 200 and 750 mm/min. Table 3 shows the yield strength $R_{p0.2}$, ultimate tensile strength R_m, uniform elongation A_g and the elongation at fracture A_{80} for both materials for the standardized testing speed and a speed of 750 mm/min.

The results show that the crystalline texture, i.e. the angle of the applied tension with respect to the RD, has a significant influence on all mechanical properties (Table 3). No matter which material is objected, the yield and ultimate tensile strength rise whereas the uniform and fracture elongations fall when the specimens are oriented perpendicular to RD. An increasing tension test speed also leads to slightly higher tension strengths and smaller uniform elongations, regardless of the specimen's orientation to RD.

The friction values of the coated material also have to be considered when a shear cutting process is numerically simulated. A strip-pull-out test was performed to obtain the coefficient of the kinetic friction in between the coated material and the tool material. The tool material used in the strip-pull-out test is the same as the material of the blank holder, punch and die of the shear cutting tool. The tests were carried out at pull-out speeds of 50, 200 and 500 mm/min. For two different contact pressures, 4 and 40 MPa, the coefficient of the kinetic friction resulted in the same value of 0.15. The value also stays the same for higher pull-out speeds and does not depend on the RD.

Table 1
Chemical composition.

Material	Alloying element in mass percent (wt%)							
	Fe	C	Si	Mn	P	S	Cr	Al
A and B	97.00	0.02	2.42	0.16	0.02	0.01	0.03	0.34

3. Experimental setup

To calibrate the fracture behavior of the materials in the FEA, shear cutting experiments were performed on an industrial mechanical single action press. In addition to the calibration experiments, specimens for the single sheet tester (SST) were produced with the same cutting tool. Fig. 2 (a) shows the schematic setup of the shear cutting tool used. The sheet metal is clamped between the blank holder and the die and is separated by the punch that travels towards the die. To prevent the tool from flattening the burr and, in this way, changing the material's stress state when small sample widths were cut, grooves were ground into the die (Fig. 2 (a)).

Important tool parameters are the relative CCL between the punch and die as well as the radii of the cutting edges of the punch and die (R_P and R_D). For the investigations within this paper, the clearance was set to 30 μm. Hence, the relative cutting clearance of material A and B results in 10% and 6% of the sheet metal thickness s_0. Two different cutting edge radii were investigated. On the one hand, a die and punch radius of 15 μm should simulate a new sharp cutting tool, while on the other hand a radius of 70 μm on both cutting edges should represent a blunt, worn tool. The surface pressure under the blank holder amounts to 300 MPa. The specimens for the single sheet measurements were produced with two different cutting velocities, 0.04 and 0.15 m/s. These two velocities correspond to a stroke speed of 60 and 200 strokes per minute. Hence the influence of the velocity is not examined within the FEA; a slow testing speed of 0.83 mm/s is used to calibrate the material model.

The influence of the cutting process on the electromagnetic properties is analyzed by increasing the length of the cutting line of the specimens for SST measurements. Fig. 2 (b) shows a processed steel sheet. The positioning system allows the strip widths to be varied in order to increase the length of the shear cutting line inside the test area of the single sheet tester. This leads directly to a bigger material volume, which is affected by the emerging residual stresses. The cut specimen widths w_S as well as the

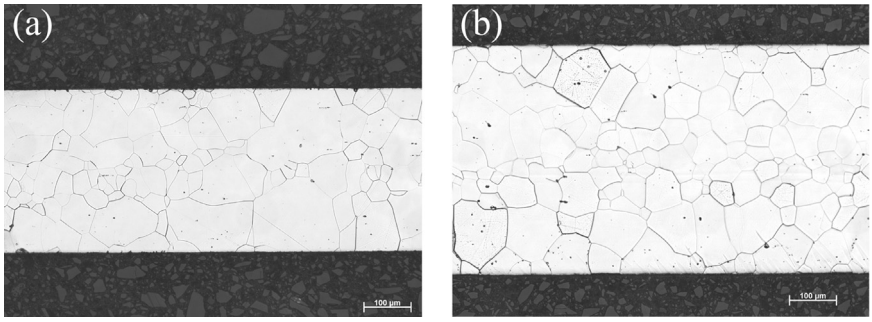

Fig. 1. Micrograph of material A (a) and material B (b).

Table 2
Metallographic analysis.

Material	A	B
Thickness (mm)	0.35	0.5
Grain diameter (µm)	51.3	47.8
Grains/thickness	7.1	11.3
Hardness ($HV_{0.2}$)	165	167

Table 3
Mechanical properties.

Material	RD (°)	v_t (mm/min)	$R_{p0.2}$ (MPa)	R_m (MPa)	A_g (%)	A_{80} (%)
A	0	Quasistatic	363	464	17.7	24.6
	0	750	369	480	16.6	24.3
	90	Quasistatic	368	487	16.3	19.7
	90	750	358	501	15.5	19.1
B	0	Quasistatic	358	471	18.5	28
	0	750	367	484	17.2	25.6
	90	Quasistatic	361	483	16.9	23
	90	750	371	497	15.5	22.7

corresponding overall length of the shear cutting line l_S are listed in Table 4. The specimens themselves must be cut to a length of 120 mm (dashed lines Fig. 2 (b)). The specimens were cut in 0° and 90° orientation so that the influence of the orientation of the cutting line relative to the RD could be studied.

In order to calibrate the FEA, the cutting force over the tool travel position and the characteristic cutting surface parameters (rollover h_R, clean-cut h_C, fracture h_F and burr height h_B, Fig. 3) following [17] are measured for each parameter configuration. The

Table 4
Specimen widths cut for the SST.

w_S (mm)	Number of samples	l_S (mm)
120	1	240
60	2	480
30	4	960
15	8	1920
10	12	2880
5	24	5760

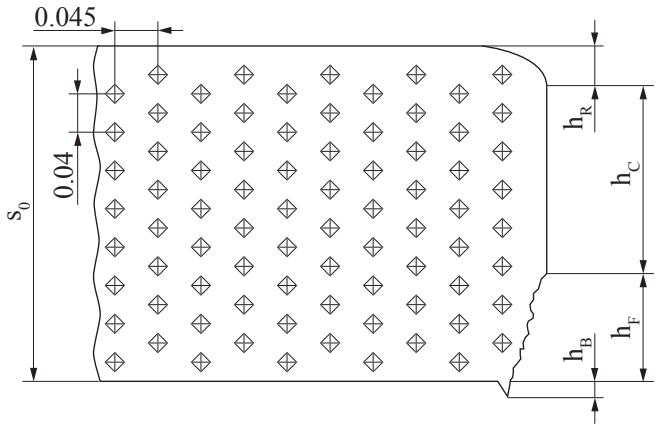

Fig. 3. Micro hardness measurement grid and characteristic cutting surface parameters h_R, h_C, h_F and h_B.

data is gathered using a tactile measurement system with an accuracy of 1µm. To understand the influences of each parameter

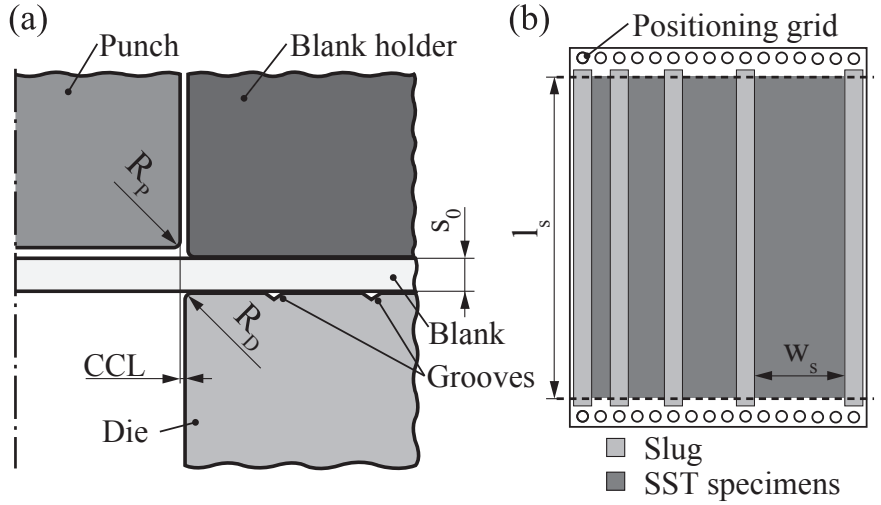

Fig. 2. (a) Draft of the shear cutting tool; (b) processed electrical steel sheet with different SST specimen widths w_S.

variation on the volume affected by work hardening within the electrical sheet, metal micro hardness measurements were taken. The applied measurement grid is shown in Fig. 3. For the investigations, a Vickers spike with a test force of 0.25N was applied.

4. Mechanical FEA setup

The experimental shear cutting setup is modeled using a two dimensional FEA. Since a symmetric cutting tool is used, a symmetrical boundary condition is implemented in the FEA. The analysis is performed with a plain strain element type CPE4R. The length of the element edges varies from 0.003 mm in the ZASC to 0.1 mm in the other blank areas. This leads to a total of 2857 elements for material A and 3083 for material B. To prevent excessive distortion of the elements in the ZASC, the Arbitrary Lagrange–Eulerian method is used every third time increment. Friction is implemented with a penalty contact.

The stress–strain data is extrapolated by a mixed swift voce approach. The ductile damage model is chosen as the damage criterion. Since the only purpose of the FEA is the qualitative investigation of the remaining residual stresses after the cutting process, the stress–strain curve as well as the damage criterion is calibrated using the measured cutting force-tool travel data and characteristic cutting surface parameters.

Each experimental process step is transferred directly to the shear cutting FEA model, ensuring a realistic model. The sequence is divided into three steps. First, the electrical sheet metal is clamped between the die and the blank holder with the same surface pressure as in the experiment. Then, the blank is cut within the second step. The last step models the pull-out process of the punch and the release of the cut part between the blank holder and the die. In this way, each stress state that is induced by external forces is removed, which allows the residual stresses left in the processed electric sheet metal to be examined.

As in the calibration experiment, the cutting speed is set to 0.83 mm/s. Due to the fact that only one CCL (30 μm) is investigated within the experimental shear cutting process, the residual stresses at two additional CCL (15 and 50 μm) are considered in the FEA at two different cutting tool radii (10 μm and 70 μm).

5. Electromagnetic test setup

The metrological characterization of a sample series with an increasing cutting line for both materials was performed on a 120 mm × 120 mm single sheet tester (SST), which is incorporated into a computer-aided setup according to the international standard IEC 60404-3. In order to study the influence of the area of cut surface related to the sample volume, samples of 120 mm × 120 mm were cut into a different number of strips with a fixed width per sample. These strips are then taped together with a non-magnetic adhesive tape to ensure that the effect of sample geometry is negligible, e.g. one strip of 120 mm, two strips of 60 mm, four strips of 30 mm, etc. A detailed overview of the strip widths investigated is given in Table 4 and Fig. 4. Samples are characterized using controlled sinusoidal magnetic flux density with a form factor error of less than 1%. Measurements were carried out under quasi-static conditions and in a frequency range from 10 Hz to 1000 Hz.

6. Mechanical experimental results

The tactile cutting surface parameter measurements show that rollover, clean cut and burr heights are much smaller when the blanks are cut with a sharp instead of a worn tool. In terms of cutting speed variation, the clean cut height slightly increases when a sharp tool is used for cutting, and slightly decreases when a blunt tool is used. These effects can be observed regardless of the sheet metal thickness and the RD. Taking a closer look at the RD, it is apparent that the rollover and clean cut height increase slightly and the fracture height marginally decreases when cutting is performed in a perpendicular direction instead of in RD. This behavior can be explained by the slight difference in mechanical material properties in and perpendicular to RD. This occurs because the deformation and fracture behavior when cutting is performed in RD is determined by the mechanical properties perpendicular to the RD, and vice versa.

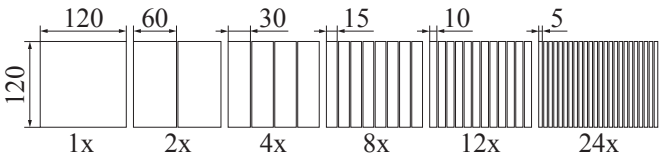

Fig. 4. Sample preparation for magnetic characterization of different proportions of cut surface per initial sample volume.

Fig. 5 shows the relative cutting surface parameters for blanks of material A that were cut in RD and 90° to RD with a sharp tool, using a cutting speed of 0.04 m/s and in 90° to RD with a blunt tool, using two different cutting speeds 0.04 and 0.15 m/s.

The cutting surface parameters shown in Fig. 5 are the median values of 42 measurements per configuration. When the distribution of the cutting surface parameters is examined more closely, a smaller deviation within the clean cut and fracture height can be discerned in Fig. 6, when the cutting tool is worn instead of sharp.

Fig. 7 displays images of the cutting surfaces for material A and B. The cutting line is oriented in RD and the cutting speed is 0.04 m/s. A higher roll over, clean cut and burr height can be observed when the tools are worn in Fig. 7 (b) and (d). The smaller deviations within the clean cut height when cutting is performed with a worn tool can also be clearly ascertained. The apparent larger blank thickness in (b) and (d) result from the higher burr. The influence of the cutting edge wear state on the characteristic structure of the ZASC can also be clearly seen when looking at the optical micrographs in Fig. 8. A worn tool leads to an increased material structure deformation.

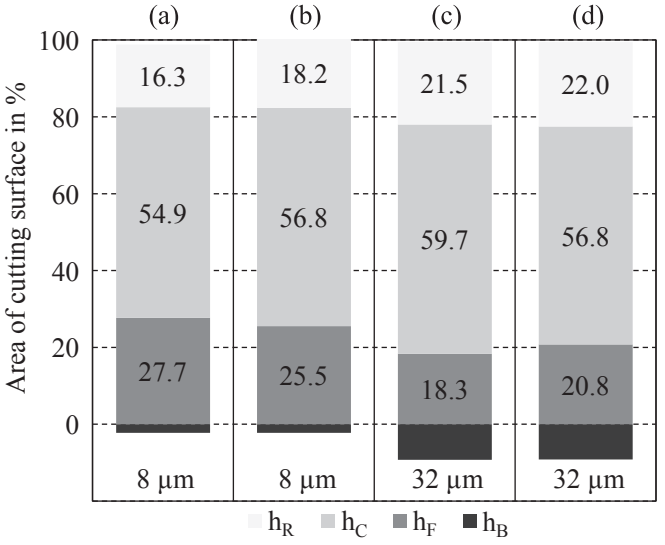

Fig. 5. Cutting surface parameters for material A; CCL 30μm; (a) sharp, 0.04m/s, 0°; (b) sharp, 0.04m/s, 90°; (c) worn, 0.04m/s, 90°; (d) worn, 0.15m/s, 90°.

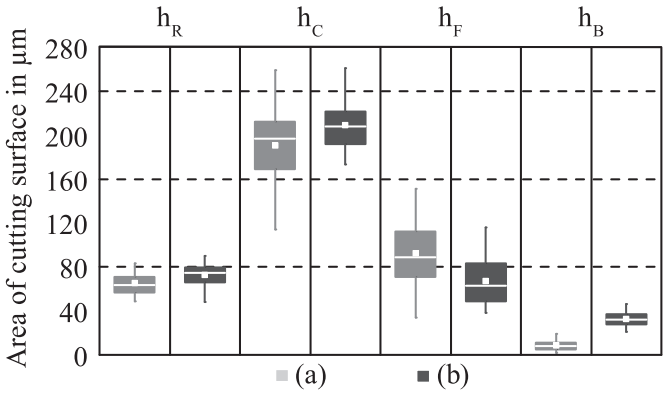

Fig. 6. Detailed cutting surface parameters for material A; CCL 30µm; (a) sharp, 0.04m/s, 90°; (b) worn, 0.04m/s, 90°.

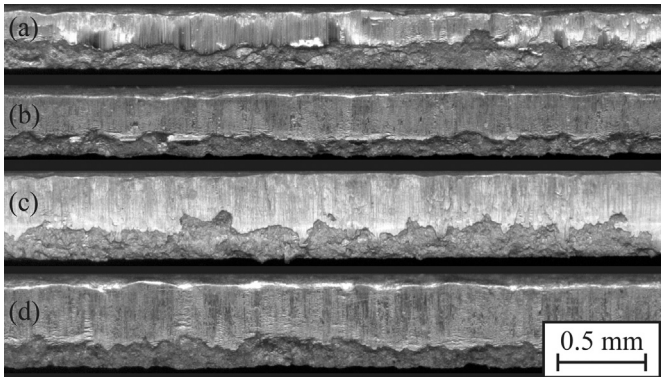

Fig. 7. Cutting surface images at two different wear states; sharp tool material A (a), material B (c); worn tool material A (b), material B (d).

Hardness measurements for material A (Fig. 9) show that a blunt cutting tool leads to an increased area that is affected by work hardening. The values in between each indentation are interpolated linearly. The black line surrounding the hardness measurement represents the cutting surface. Due to the small distances from the part edge it is often impossible to make every indentation (Fig. 3) without risking a damage of the indenter. The local Vickers Hardness values are always referred to the hardness values of the virgin material ($H_0 = 171\ HV_{0.2}$). It is apparent that the hardness does not only vary the closer the indentations are to the clean cut but also over the blank thickness.

A mean of all hardness values that have the same distance from the cutting edge simplifies the comparison between the parameter variations investigated. Fig. 10 depicts an average of three hardness measurements for material A cut with sharp and worn cutting edges in and perpendicular to the RD at two different speeds. Regardless of the thickness and the RD, the material is affected by higher strain hardening, and furthermore, the plastically-deformed zone reaches further into the material when a blunt tool is used. When cutting operations in and transverse to RD are compared, only a small difference can be determined, which also originates from the different mechanical properties.

The plastically-deformed zone is also increased when cutting is performed at higher velocities. When compared to the influence of tool wear state, the impact of velocity variation is smaller. The largest extent of the plastically-deformed area is reached when the electric steel sheet is cut at 0.15 m/s using a blunt cutting tool. Low speed and sharp tools minimize the area affected by work hardening. As seen in Fig. 10, the impact of the orientation of the cutting line to the RD is quite small.

7. Mechanical FEA results

The FEA provides the stress distribution inside the ZASC. When analyzing these stresses it is important to display the stresses in a way that enables comparison of the different results. It is not expedient to analyze the residual stress by means of an equivalent stress such as $\sigma_{v.Mises}$, because it is not possible to distinguish between tensile and compression stresses. Fig. 11. shows a shear cutting simulation of material A in RD with a worn tool and a CCL of 50µm. The distribution of the stresses σ_1 (a), σ_2 (c) and the shear stress σ_{12} (b) illustrates that certain areas undergo different distortions to others. In this case, 1 and 2 correlate to the global coordinate system. In the area near the cut edge, where the fracture starts, one can see high compression and tension stresses σ_2. In the roll-over area and on the lower edge of the blank we can see the same effect for σ_1. Compression stresses in 1 and 2 directions are located in the middle of the blank. Compared to the stresses σ_1 and σ_2, the shear stress σ_{12} is quite small. For electromagnetic considerations, the analysis of von Mises stress is insufficient, because it is not possible to differentiate between tension and compressive residual stresses. This differentiation, however, is essential because tensile and compressive stresses affect the electromagnetic properties to different extents, according to [18,19]. To minimize the effort needed to compare the parameter variations to each other, the mixed stress value $\sigma_{MAX,ip,abs.}$ (d) is used. Here, the highest local in-plane absolute principal stress is chosen. The algebraic sign is not considered in the selection but in the presentation of the results.

Fig. 12 shows the influence of a variation of the CCL and cutting edge condition for material B. In (a) and (b) the CCL is 10µm and in

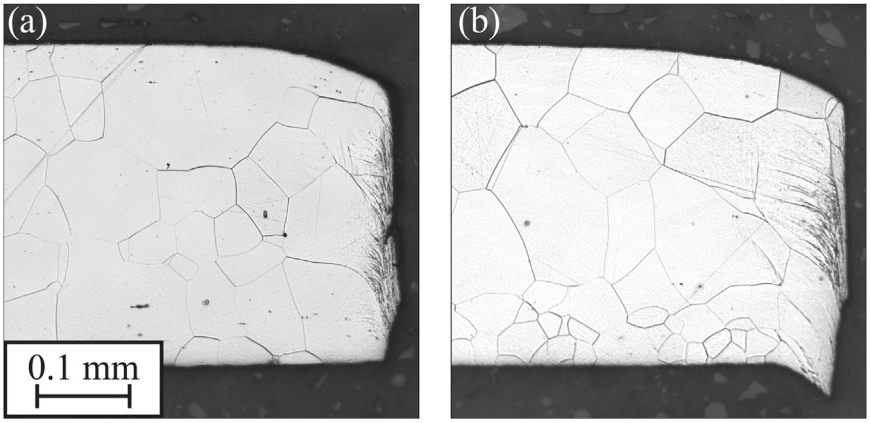

Fig. 8. Micrograph perpendicular to the cutting surface of material A cut with a sharp (a) and blunt (b) cutting tool.

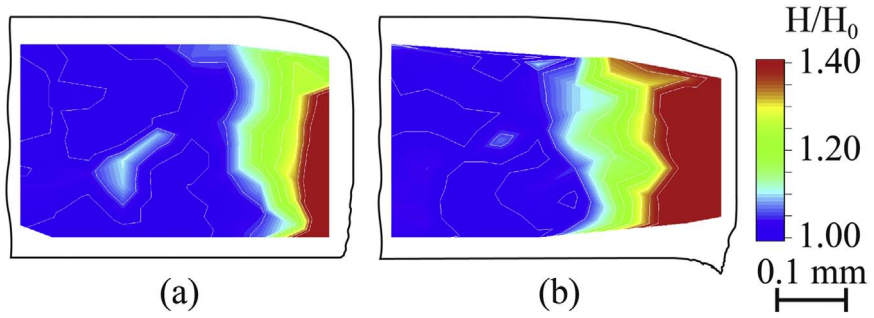

Fig. 9. Normalized micro hardness measurement in the ZASC for material A; CCL 30 μm; (a) sharp, 0.04 m/s, 90°; (b) worn, 0.04 m/s, 90°.

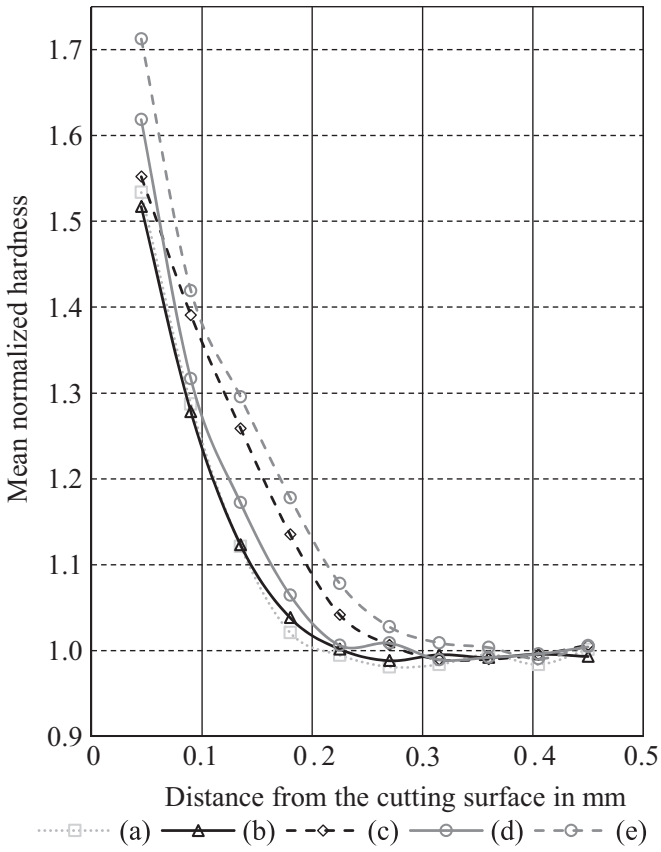

Fig. 10. Mean normalized micro hardness measurement for material A; CCL 30 μm; (a) sharp, 0.04 m/s, 0°; (b) sharp, 0.04 m/s, 90°; (c) worn, 0.04 m/s, 90°; (d) sharp, 0.15 m/s, 90°; (e) worn, 0.15 m/s, 90°.

(c) and (d) the CCL is set to 30μm. The tool edge condition is sharp in (a) and (c). In (b) and (d) a worn cutting tool is used.

The penetration depth of the residual stresses in the ZASC can be reduced significantly when cutting with small CCLs. When a sharp instead of a worn tool edge is used, the penetration depth can also be reduced. Compared to (a) and (c) the absolute stresses and the area affected by residual stresses in (b) and (d) is larger. These tendencies stay the same regardless of the alignment of the cutting line to the RD or the sheet metal thickness.

A simplified analysis of the stress distribution is shown in Fig. 13. Like in the analysis of the hardness measurements, a mean $\sigma_{MAX,ip,abs.}$ value across the sheet metal thickness (white lines in Fig. 12) is calculated.

In this case, we also distinguish between compression and tension stresses. One can see that both small cutting CCLs, as well as sharp tools, reduce the extent of the ZASC. When a blunt cutting edge and a large CCL is used, the tension residual stresses reach up to 900 μm deep into the material.

Fig. 14 depicts the influence of the cutting edge condition for large CCL for material A in 90° to RD. For a CCL of 50μm the extend of the ZASC stays the same regardless of the cutting edge condition.

8. Electromagnetic test results

The magnetic properties of the material studied deteriorate as the proportion of cutting line per sample increases, i.e. with decreasing strip widths. The magnetization curve is shifted to higher magnetic field strengths, Fig. 15 (a) and specific losses increase (b). Even though non-oriented (NO) electrical steel is supposed to have a homogenous isotropic microstructure and texture, distinctly anisotropic behavior can be observed, as for most NO materials. Magnetic behavior in RD (0°) is beneficial when compared to the behavior in a transverse direction (90°) with lower losses and lower magnetic field strength required to achieve a certain polarization. For magnetization behavior, the range between 0.5 T and 1.5 T is particularly crucial, whereas in saturation the effect of cutting diminishes. However, relative loss deterioration increases constantly with higher polarizations. Fig. 15 (b) further shows the influence of the sheet thickness on the losses. For material A (0.35 mm), losses at 100 Hz are lower than for material B (0.5 mm) due to the influence of sheet thickness on the classical eddy current losses, which decrease with decreasing sheet thickness. These general coherences pertain to all investigated sets of cut parameter combinations, i.e. sharp/worn tools with a speed of 0.04 m/s and 0.15 m/s.

The effect of different cutting parameters on the magnetic behavior with samples of decreasing strip width can be deducted from Fig. 16. Variations of cutting parameters influence the magnetic properties to a different extent. An increasing cutting speed and wear of the tool affect losses and the required magnetization to reach a certain polarization negatively. The effect is more pronounced for increasing amounts of cut edge per sample (Fig. 16 (a)). However, magnetization behavior is affected to a far greater extent than losses. Fig. 16 (b) and (c) illustrate this behavior. For 120 mm strips all B–H-hysteresis loops are congruent irrespective of the cutting speed and wear state of the tool. For 5 mm strips the hysteresis loops shear to higher magnetization. Concurrently with a shearing of the hysteresis loop the remanence polarization decreases, whereas the coercivity increases. This results in a significantly higher magnetization while the overall size of the hysteresis loop remains mainly unaffected. The wear state of the tool is more detrimental than an increased cutting speed. Samples of material A (90°) show analogous behavior as the exemplarily depicted diagrams of Fig. 16 for Material B (0°).

Magnetic characterization was performed in a quasistatic manner, as well as with frequencies up to 1000 Hz. Fig. 17 (a) shows the absolute values for specific losses with

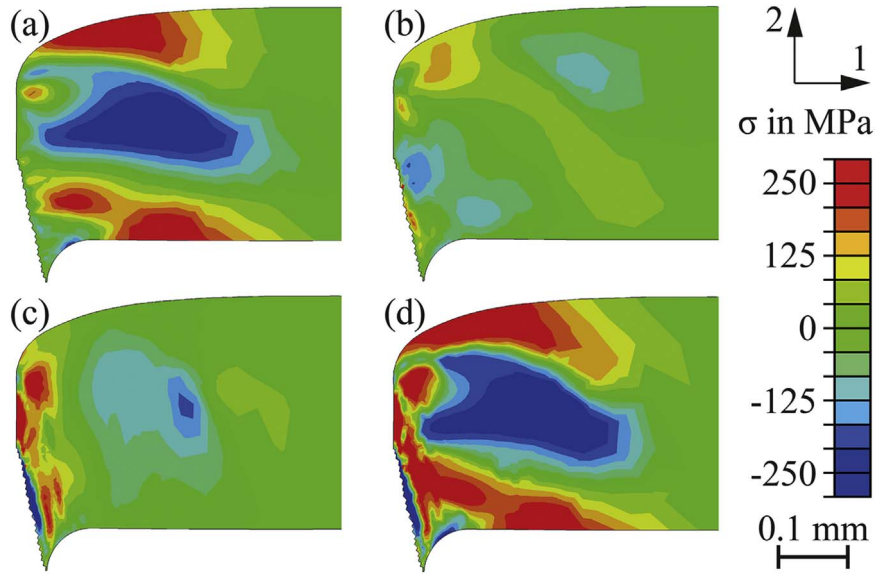

Fig. 11. Residual stress distribution for material A with a blunt tool, a CCL of 50 μm and in 90° to RD; (a) σ_1; (b) σ_2; (c) σ_{12}; (d) $\sigma_{MAX,ip,abs.}$

increasing frequency and decreasing strip widths. At 750 Hz, losses are between 60 and 80 W/kg, compared to 1.4–2.0 W/kg at 50 Hz. A deeper analysis of the loss increase as a result of an increasing cutting line can be obtained by examining normalized losses. Normalized losses (b), i.e. relative loss, increase for smaller strip widths compared with the 120 mm sample at given frequency. In addition, the relative deterioration decreases with increasing frequency. This behavior illustrates that cutting influences primarily the static loss components, i.e. hysteresis losses, whereas the influence on dynamic loss components is significantly lower. Furthermore, the extent of deterioration, up to 60% (worn, 0.15 m/s) is noteworthy considering that actual motor geometries, e.g. tooth sizes, can include even geometries with dimensions smaller than 5 mm.

The behavior observed for relative deterioration of losses is similar for all sample series, e.g. materials A and B, 0° and 90° and different speed and wear of the tool. By way of example, values for the influence of a tool's wear state, for both materials in rolling as well as in transverse direction, is given in Table 5. The values lie in comparable ranges. For 50 Hz, the lowest deterioration for 5 mm strips compared with 120 mm strips is 1.33 (0.35 mm, 0.04 m/s, sharp). The data from Table 5 suggests that the tool's wear state has a more detrimental effect on losses in RD (5–6%) than in transverse direction (1–2%). This highlights the complexity of the interdependence between different effects. In this case, the behavior may be due to the texture in combination with the distribution of residual stresses as a result of cutting. Material parameters, as for example the magnetostriction, depend on the crystal orientation. Furthermore, magnetostriction for a given silicon content of 2.4 wt% has a different sign in the [100] and [111] direction [20]. The macroscopic behavior in one spatial direction thus depends on the textural distribution of these orientations. According to [5], the behavior of a material under stress depends on the stress tensor and the magnetostriction. Magnetization in the direction of the applied stress increases if the two terms, magnetostriction constant and stress tensor, have the same sign. In the observed case, losses increase in both spatial directions. However, the comparison of a sharp and a worn tool shows a more detrimental effect in RD for both sheet thicknesses.

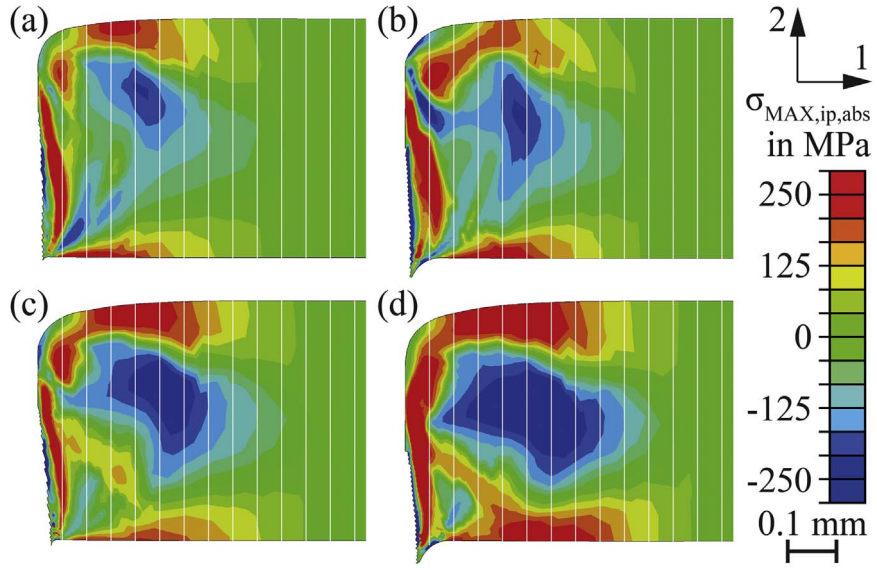

Fig. 12. Residual stress distribution for material B in 90° to RD; (a) 10μm CCL, sharp tool; (b) 10μm CCL, worn tool; (c) 30μm CCL, sharp tool; (d) 30μm CCL, worn tool.

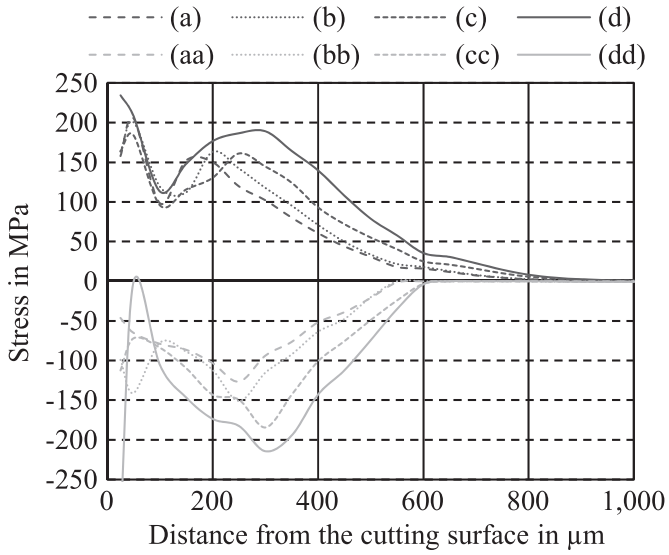

Fig. 13. Tension and compression mean residual stress over sheet thickness for material B in 90° to RD; (a)/(aa) 10µm CCL, sharp tool; (b)/(bb) 10µm CCL, worn tool; (c)/(cc) 30µm CCL, sharp tool; (d)/(dd) 30µm CCL, worn tool.

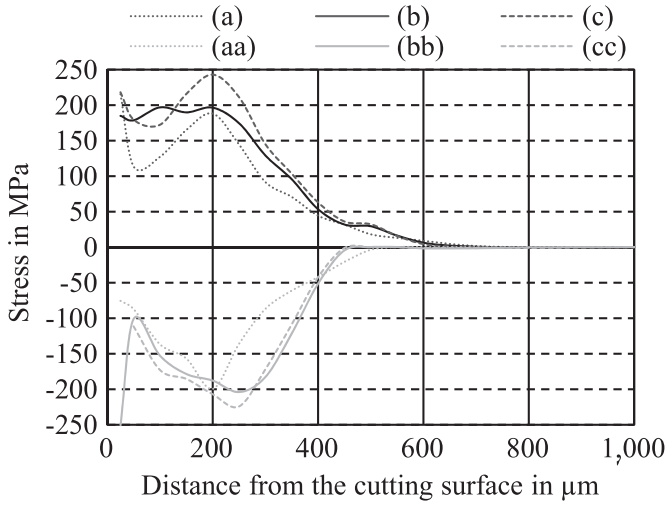

Fig. 14. Tension and compression mean residual stress over sheet thickness for material A in 90° to RD; (a)/(aa) 10µm CCL, worn tool; (b)/(bb) 50µm CCL, worn tool; (c)/(cc) 50µm CCL, sharp tool.

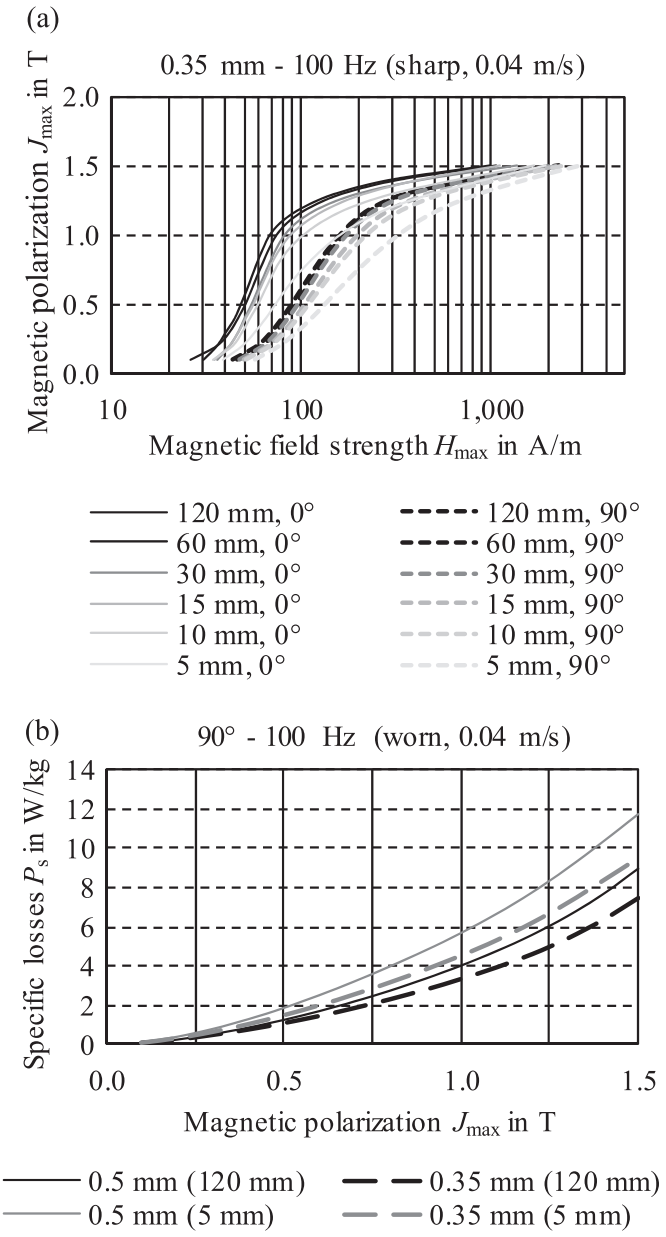

Fig. 15. (a) Magnetization in 0° and 90° for material A; (b) specific losses for different sheet thicknesses.

9. Conclusions

In-depth studies of the correlations between FEA and electromagnetic properties after shear cutting enable us to predict the magnetic and mechanical behavior of NO electrical steel in its final geometry with respect to the cutting parameters.

In this research the results gathered show that a sharp tool edge always leads to better results than a worn cutting edge. This applies whether we look at the increase of the clean cut height, plastically-deformed area, specific losses or residual stresses. In addition, the experiments show that high cutting speeds lead to a larger strain-hardened area, which, in turn, gives rise to higher residual stresses and losses. The FEA of the CCL influence showed that smaller cutting clearances may lead to higher residual stresses right next to the cutting surface, but they also reduce the penetration depth.

Due to the effects of size, the deformation and fracture behavior of electrical steel differs from that of standard steels [21]. Next to a transcrystalline deformation and fracture behavior, the large grain size of around 100 µm supports intercrystalline material deformation and fracture behavior. This results in high deviations when we look at the cutting surface parameters. Thus, when materials with different chemical composition, heat treatment and mechanical properties are compared, an analysis of the cutting surface parameters may not lead to satisfying results, because of the high deviations.

The FEA of the shear cutting process is a useful tool for the qualitative residual stress prediction when the influence of the CCL and tool wear state on the electromagnetic properties of electric sheet metal is investigated. The analysis also confirms the experimental results, showing that the residual stresses rise with increasing wear on the cutting edges. Nevertheless, the computational analysis at elevated cutting speeds is difficult to realize because, in addition to the material behavior at high strain rates, the behavior at high temperatures has to be implemented into the FEA model.

When the hardness and residual stress distributions are viewed more closely, two things can be noticed. On the one hand, it is

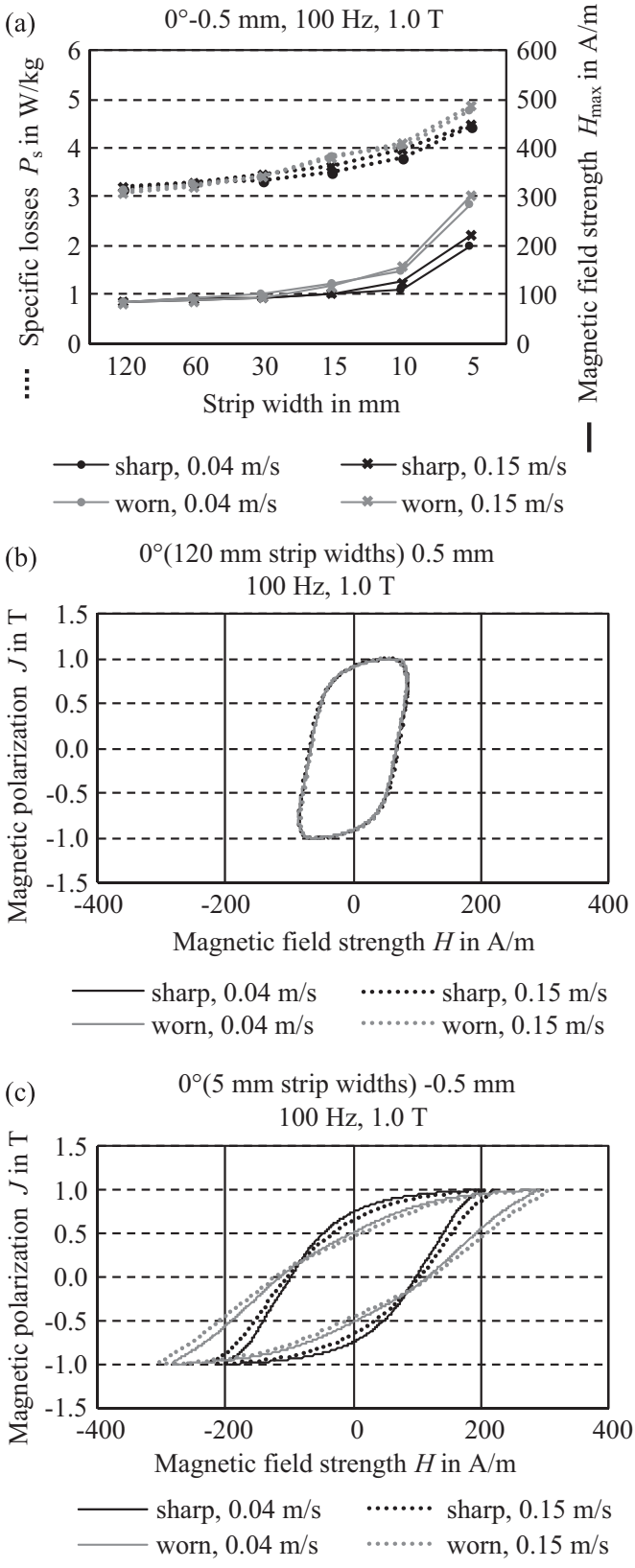

Fig. 16. Influence of different cutting parameters on the magnetic properties for material B, 0°; (a) losses and magnetization; (b) B–H-loops for 120 mm strip widths; (c) B–H-loops for 5 mm strip widths.

clear that the penetration depth of the residual stresses always exceeds the penetration depth of the strain-hardened area. However, a qualitative analysis in between each cutting parameter

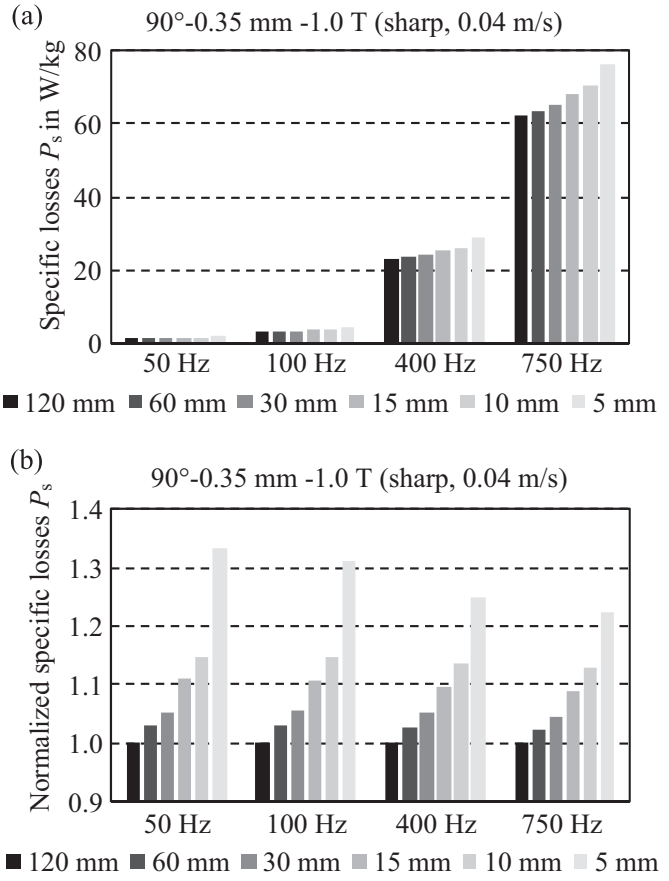

Fig. 17. Losses for different strip widths at increasing frequency for material A (0.35 mm sheet thickness) (a) absolute losses, sharp, 0.04 m/s, 90°; (b) normalized losses, sharp, 0.04 m/s, 90°.

Table 5
Relative loss deterioration for 5 mm strip widths compared to 120 mm strip widths.

		Sharp 0.04 m/s 50 Hz	Worn 0.04 m/s 50 Hz
Material A	0°	1.33	1.38
	90°	1.44	1.46
Material B	0°	1.44	1.60
	90°	1.44	1.45

configuration is still possible. On the other hand, it is apparent from the distributions that the stress and hardness values are not constant over the blank thickness and over the whole penetration depth. Hence, a MOKE and hardness analysis performed in a plane parallel to the blank surface are only representative when the distance from the surface in question to the blank surface is known. And even if the distance is known, the maximum residual stresses might not be located in the surface observed, especially when different separation techniques and processing parameters are under consideration.

The results of the electromagnetic characterization display a steady rise in specific losses with increasing cutting line length for all observed sample series, i.e. regardless of the orientation of the cutting line relative to the RD, blank thickness or cutting process parameter settings. Although, the material studied is a NO grade, the magnetic behavior, e.g. losses and magnetization, displays considerable anisotropic behavior. This anisotropy is also exhibited for the mechanical properties in the form of higher values for $R_{p0.2}$ and R_m, as well as lower values for A_g and A_{80} in 90° direction.

Anisotropic effects can be directly linked to the material's texture. Even though a final annealing treatment after cold rolling ensures a recrystallized microstructure, various research shows that textures are inherited from preceding processing steps [15,22]. Magnetostriction constants of single crystals depend on the magnetization vector relative to the crystal orientation [20]. Thus, the global magnetostrictive behavior of a polycrystal depends on the distribution of all orientations within the material, i.e. the crystallographic texture. Interrelated effects of mechanical stress and magnetostriction can result in either a shearing or steepening of the B–H-Hysteresis loop [5]. Shearing generally causes a deterioration of magnetic properties, as observed within this research.

In their entirety, the results indicate that changes in the electromagnetic deterioration between sample series stem from differences in the residual stress state after cutting, because materials A and B are comparable in chemical composition, grain sizes, hardness and microstructure. Sheet thickness and cutting parameters alter the stress state and the structure near the cut edge. The wear state of the cutting edge, as well as the cutting speed, have an influence on the resulting magnetization. The analysis of normalized specific losses at different frequencies affirms that cutting primarily affects the hysteresis losses and, therefore, the detrimental effects of cutting are graver at low frequencies.

10. Future outlook

The residual stress and hardness analysis show that a review of the mean values over the blank thickness along the distance from the cutting surface is sufficient to evaluate each cutting parameter configuration. Hence an analysis of the cutting influence on the electromagnetic material properties using the nGI is a good method for analyzing this interdependence at different magnetic field strengths, without changing the residual stress state of the test specimen when preparing a micrograph. In addition to the advantage that the residual stress state in the specimen is not changed by a preparation step, the nGI allows very small residual stress changes to be detected. [3] shows that even a small cutting parameter variation can be detected. For this reason, an investigation of the interdependence of different shear cutting parameters and the resulting electromagnetic properties will be performed using the nGI. Further studies on the precise combinatory effects of residual stresses and microscopic magnetic processes needs to be conducted in order to deduct the relations to global behavior.

Further to an investigation of the electromagnetic influence of the shear cutting process, the mechanical material behavior throughout the deformation and fracture process has to be analyzed. The influence of size effects on the shear cutting process is widely unknown. Firstly, the material failure behavior has to be investigated. Cutting large grains not only leads to a mixed trans- and intercrystalline fracture behavior, but also increases the cutting force. Secondly, the temperature in between the two cutting edges will rise when smaller blank thicknesses are cut, because of the smaller material that can transfer the heat into the connecting material regions and the reduced cutting time.

Acknowledgement

This work is supported by the DFG and carried out in the research group project “FOR 1897 – Low-Loss Electrical Steel for Energy-Efficient Electrical Drives”.

References

[1] M. Emura, F.J.G. Landgraf, W. Ross, J.R. Barreta, The influence of cutting technique on the magnetic properties of electrical steels, J. Magn. Magn. Mater. (2003) 358–360, http://dx.doi.org/10.1016/S0304-8853(02)00856-9.
[2] H. Naumoski, B. Riedmüller, A. Minkow, U. Herr, Investigation of the influence of different cutting procedures on the global and local magnetic properties of non-oriented electrical steel, J. Magn. Magn. Mater. (2015) 126–133, http://dx.doi.org/10.1016/j.jmmm.2015.05.031.
[3] R. Siebert, J. Schneider, E. Beyer, Laser cutting and mechanical cutting of electrical steels and its effect on the magnetic properties, IEEE Trans. Magn. 4 (2014) 1–4, http://dx.doi.org/10.1109/TMAG.2013.2285256.
[4] G.E. Totten, M.A.H. Howes, T. Inoue, Handbook of Residual Stress and Deformation of Steel, 2002.
[5] R.M. Ferromagnetism, Bozorth, 1978.
[6] M. LoBue, C. Sasso, V. Basso, F. Fiorillo, G. Bertotti, Power losses and magnetization process in Fe–Si non-oriented steels under tensile and compressive stress, J. Magn. Magn. Mater. (2000) 124–126, http://dx.doi.org/10.1016/S0304-8853(00)00092-5.
[7] A.J. Moses, A. Ntatsis, T. Kochmann, J. Schneider, Magnetostriction in non-oriented electrical steels, J. Magn. Magn. Mater. (2000) 669–672, http://dx.doi.org/10.1016/S0304-8853(00)00254-7.
[8] R. Rygal, A.J. Moses, N. Derebasi, J. Schneider, A. Schoppa, Influence of cutting stress on magnetic field and flux density distribution in non-oriented electrical steels, J. Magn. Magn. Mater. (2000) 687–689, http://dx.doi.org/10.1016/S0304-8853(00)00259-6.
[9] T. Nakata, M. Nakano, K. Kawahara, Effects of stress due to cutting on magnetic characteristics of silicon steel, IEEE Transl. J. Magn. Jpn. 6 (1992) 453–457, http://dx.doi.org/10.1109/TJMJ.1992.4565422.
[10] H. Cao, L. Hao, J. Yi, X. Zhang, Z. Luo, S. Chen, R. Li, The influence of punching process on residual stress and magnetic domain structure of non-oriented silicon steel, J. Magn. Magn. Mater. (2016) 42–47, http://dx.doi.org/10.1016/j.jmmm.2015.12.098.
[11] T. Belgrand, S. Eple, Tell us about your punch, we'll tell you about your electrical steel magnetic properties, J. Phys. IV PR2 (1998) Pr2-611, http://dx.doi.org/10.1051/jp4:19982141.
[12] P. Baudouin, M. De Wulf, L. Kestens, Y. Houbaert, The effect of the guillotine clearance on the magnetic properties of electrical steels, J. Magn. Magn. Mater. 1–3 (2003) 32–40, http://dx.doi.org/10.1016/S0304-8853(02)00004-5.
[13] Karl Heinz Schmidt, Influence of punching on the magnetic properties of electric steel with 1% silicon, J. Magn. Magn. Mater. 1–3 (1975) 136–150, http://dx.doi.org/10.1016/0304-8853(75)90116-X.
[14] S. Steentjes, D. Franck, K. Hameyer, S. Vogt, M. Bednarz, W. Volk, J. Dierdorf, G. Hirt, V. Schnabel, H.N. Mathur, S. Korte-Kerzel, On the effect of material processing: microstructural and magnetic properties of electrical steel sheets, 2014, 1–7. http://dx.doi.org/10.1109/EDPC.2014.6984436.
[15] S. Steentjes, N. Leuning, J. Dierdorf, X. Wei, G. Hirt, H.A. Weiss, W. Volk, S. Roggenbuck, S. Korte-Kerzel, A. Stoecker, R. Kawalla, K. Hameyer, Effect of the interdependence of cold rolling strategies and subsequent punching on magnetic properties of NO steel sheets, IEEE Trans. Magn. (2016) 1, http://dx.doi.org/10.1109/TMAG.2016.2516340.
[16] CEN European Committee for Standardization. Metallic Materials – Tensile testing – Part 1: Method of Test at Room Temperature, FprEN ISO 6892-1, 2016.
[17] VDI-Department of Production and Manufacturing. VDI 2906 – Quality of cut faces of (sheet) metal parts after cutting, blanking, trimming or piercing, VDI 2906, 2016.
[18] V. Permiakov, L. Dupré, A. Pulnikov, J. Melkebeek, Loss separation and parameters for hysteresis modelling under compressive and tensile stresses, J. Magn. Magn. Mater. (2004) E553, http://dx.doi.org/10.1016/j.jmmm.2003.11.381.
[19] N. Leuning, S. Steentjes, M. Schulte, W. Bleck, K. Hameyer, Effect of elastic and plastic tensile mechanical loading on the magnetic properties of NGO electrical steel, J. Magn. Magn. Mater. (2016) 42–48, http://dx.doi.org/10.1016/j.jmmm.2016.05.049.
[20] H.P.J. Wijn, G. Bertotti, F. Fiorillo, Magnetic Alloys for Technical Applications. Soft Magnetic Alloys, Invar and Elinvar Alloys, Landolt-Börnstein - Group III Condensed Matter 1994 http://dx.doi.org/10.1007/b91565.
[21] F. Vollertsen, D. Biermann, H.N. Hansen, I.S. Jawahir, K. Kuzman, Size effects in manufacturing of metallic components, CIRP Annals - Manufacturing Technology 58-2, 2009, 566–587, http://dx.doi.org/10.1016/j.cirp.2009.09.002.
[22] H. Pan, Z. Zhang, J. Xie, Preparation of high silicon electrical steel sheets with strong 51006 recrystallization texture by the texture inheritance of initial columnar grains, Metall. Mater. Trans. A. 5 (2016) 2277–2285, http://dx.doi.org/10.1007/s11661-016-3371-4.